

Introducing Electrified Vehicle Dynamics in Traffic Simulation

Transportation Research Record
2020, Vol. 2674(9) 776–791
© National Academy of Sciences:
Transportation Research Board 2020
Article reuse guidelines:
sagepub.com/journals-permissions
DOI: 10.1177/0361198120931842
journals.sagepub.com/home/trr



**Yinglong He¹, Michail Makridis^{2,3}, Konstantinos Mattas²,
Georgios Fontaras², Biagio Ciuffo², and Hongming Xu¹**

Abstract

Many studies have highlighted the added value of incorporating vehicle dynamics into microsimulation. Such models usually focus on simulation of conventional vehicles, failing to account for the acceleration dynamics of electrified vehicles that have different power characteristics from those of internal combustion engine vehicles (ICEV). In addition, none of them have explicitly dealt with the vehicle's deceleration characteristics. Although it is not commonly considered critical how a vehicle decelerates, unrealistic behaviors in simulations can distort both traffic flow and emissions results. The present work builds on the lightweight microsimulation free-flow acceleration (MFC) model and proposes an extension, marking the first attempt to address these research gaps. First, a comprehensive review of dynamics-based car-following (including free-flow) models is conducted. Second, the methodology of the MFC model to capture the dynamics of electrified vehicles is described. Then, the experimental setup in different dimensions is introduced for the model validation and implementation. Finally, the results of this study indicate that: (1) the acceleration and deceleration potential curves underlying the MFC model can accurately represent real dynamics of electrified vehicles tested on the chassis dynamometer; (2) smooth transitions can be guaranteed after implementing the MFC model in microsimulation; (3) when reproducing the on-road driving trajectories, the MFC model can deliver significant reductions in root mean square error (RMSE) of speed (by ~69%) and acceleration (by ~50%) compared with benchmarks; (4) the MFC model can accurately predict the vehicle 0–100 km/h acceleration specifications, with RMSE 49.4% and 56.8% lower than those of the Gipps model and the intelligent driver model (IDM), respectively.

Developing mathematical models to reproduce accurately vehicles' realistic longitudinal acceleration behavior is important for a wide range of scientific and industrial processes, especially considering the significant impacts of the real driving emissions test on the design of automotive applications and of future regulation of road vehicle emissions (1, 2). Transportation systems comprise many complex elements (vehicles, infrastructure, drivers, control systems, etc.) that might interact with each other (3). The interactions within such systems introduce high stochasticity (4), which in some cases makes the production of quantifiable results difficult or even impossible. Consequently, simplistic behavioral car-following models such as the Gipps model and the intelligent driver model (IDM) are usually preferred, because of their reduced computational complexity which makes them ideal for large microsimulation studies. However, modeling based on vehicle dynamics has attracted considerable interest lately. According to Ciuffo et al. (5), although behavioral models can correctly replicate traffic dynamics, their capability to reproduce vehicle dynamics and their consequent assessments on emissions and energy consumption

are questionable. Recently, lightweight models have been proposed that are quite accurate in reproducing vehicle dynamics, and lightweight enough to be used in large-scale microsimulations, such as the Fadhloun-Rakha model (6) and the microsimulation free-flow acceleration (MFC) model (7). There is still room for improvement, however. For example, recent studies show that the relation between fuel consumption and average speed for internal combustion engine vehicles (ICEV) is questionable for plug-in electric vehicles, for which higher energy consumption is related to free-flow test cases (8). Thus, more fundamental and explicit characterization of system dynamics in the car-following models is not only

¹Department of Mechanical Engineering, University of Birmingham, Birmingham, UK

²Directorate for Energy, Transport and Climate Change, European Commission – Joint Research Centre, Ispra, Italy

³Institute for Transport Planning and Systems, Department of Civil, Environmental and Geomatic Engineering, ETH Zürich, Zürich, Switzerland

Corresponding Author:

Biagio Ciuffo, biagio.ciuffo@ec.europa.eu

essential but also mandatory for the provision of reliable and robust conclusions. Moreover, the validity and suitability of a certain car-following model for engineering applications depends on capturing the observed driving and traffic behaviors with the smallest number of calibration parameters.

Mathematical expressions of state-of-the-art car-following models generally comprise two branches (9–11): (a) the free-flow branch, regulating the subject vehicle on a free road, which asymptotically approaches its desired speed; and (b) the vehicle interaction branch, governing the subject vehicle in congested conditions, where rear-end collision and traffic instability need to be avoided. Over the past few decades, various car-following models have been developed to generate vehicle trajectories that mimic empirical driving behavior as realistically as possible (6). Several systematic reviews of widely used car-following models have been undertaken (5, 12–14).

Based on whether vehicle dynamics are explicitly involved in their expressions, the models observed in the literature can be categorized into two groups: kinematics-based and dynamics-based. First, the kinematics-based (or behavioral) models, such as the Gipps model (10), the intelligent driver model (IDM) (11), the Newell model (15), and the Gazis-Herman-Rothery model (16), attempt to replicate the empirical vehicle acceleration behavior during driving. These models suffer from a notable methodological weakness, however; namely, they ignore the mechanical characteristics of the vehicle. Second, the dynamics-based models, for example, the Searle model (17), the Rakha-Pasumarty-Adjerid model (18), the Fadhloun-Rakha model (6), and the MFC free-flow model (7), explicitly incorporate vehicle dynamics into their mathematical expressions to ensure that vehicle accelerations are realistic. However, it is questionable whether such models are lightweight and flexible enough to be used in large microscopic simulation studies. The following paragraphs trace the development of dynamics-based models.

As summarized in Table 1, the dynamics-based car-following model has been a growing field across several disciplines in recent years, and relevant publications remain few, almost all of them focused on the conventional ICEV, powered by a gasoline or diesel internal combustion engine with a multi-ratio transmission. The work of Searle et al. (17) remains crucial to our wider understanding of this area. However, their proposed model assumed that the engine power at full-load operating conditions (P_e^{FL}) was constant and equal to the peak engine power (P_e^{\max}). Also, the specific dynamics of the internal driveline (e.g., transmission and engine accessories) and external resistances (i.e., aerodynamic, rolling, and grade) were not considered; instead, their effects on the power losses were all incorporated into a constant

η_a , the acceleration efficiency. Moreover, driving behavior, that is, how the driver utilizes the vehicle's full power capabilities, was not indicated, thus, the model's output was the maximum acceleration characteristics. In the subsequent study by Rakha et al. (19) the enhanced model accounted for detailed dynamics of the driveline and the resistances. Although the full-load engine power was still constant, the tractive force was upper bounded by the maximum force that can be sustained between the vehicle wheels and the roadway surface. Rakha et al. (20) then developed a variable power dynamics model in 2002 by introducing a power adjustment factor β , which dealt with the full-load power reduction caused by the effect of successive gear shifting at low speed. The factor β is a ramp function (with a positive intercept) of vehicle speed v_i , when $v_i \leq v_p$ (v_p is the speed at which maximum power occurs).

Rakha et al. (21) were the first of many who have attempted to capture typical driving behavior and vehicle dynamics at the same time. The typical acceleration output was achieved by introducing an acceleration reduction factor w_{db} , which denotes the ratio of the driver's real acceleration to the vehicle's theoretical capability. On the other hand, the model proposed in 2009 by Rakha et al. (18) adopted a power reduction factor t_{db} aiming to represent the percentage of the throttle opening, thus the power delivered from the engine can be assumed to be equal to a constant percentage of the engine power at full-load conditions. Additionally, to capture the interaction of vehicles in the traffic flow, the model considered two speed constraints: $v_{ca}^{\lim}(v_i^p, s_i)$ to avoid any collisions with the preceding vehicle and $v_{ts}^{\lim}(V_D, s_i)$ to maintain cruising in the steady-state traffic stream. Rakha et al. (22) developed the first model that explicitly captures the dynamics of engine power and gearshift. This research is critical, given that the full-load engine power P_e^{FL} during driving cannot be assumed to be constant over the entire vehicle speed range nor to be adjusted by a ramp function $\beta(v_i)$ at the low-speed region. In fact, it is well known that the engine power at full-load conditions varies as a function of the current vehicle speed v_i and the engaged gear ratio φ_g . Moreover, the gearshift behavior (w_{gb}) in this model was designed as per a fixed engine speed threshold.

The above three typical acceleration models reported by Rakha et al. however, reproduce the driving behavior (w_{db} or t_{db}) and the gearshift behavior (w_{gb}) using constant factors, thus they provide limited information in relation to each driver's unique pattern of driving. Recognizing this deficiency, an enhancement proposed in 2015 by Fadhloun et al. (23) made the model representative of different driving patterns. The basic idea behind their research is to employ a variable throttle opening t_{db} as a function of the vehicle speed v_i and the driver's

Table 1. The Development of Dynamics-Based Car-Following Models

Model (source)	Engine power ^a	Driveline and resistances	Gearshift behavior ^b	Driving behavior ^c	Collision avoidance ^d	Traffic stability ^d	Model output
Searle et al. (17)	\times, P_e^{\max}	\times	\times	\times	\times	\times	Maximum acceleration
Rakha et al. (19)	\times, P_e^{\max}	\checkmark	\times	\times	\times	\times	
Rakha et al. (20)	$\times, \beta(v_i) \cdot P_e^{\max}$	\checkmark	\times	\times	\times	\times	
Rakha et al. (21)	$\times, \beta(v_i) \cdot P_e^{\max}$	\checkmark	\times	\checkmark, w_{db}	\times	\times	Typical acceleration
Rakha et al. (18)	$\times, \beta(v_i) \cdot P_e^{\max}$	\checkmark	\times	\checkmark, t_{db}	$\checkmark, v_{ca}^{\lim}(v_i^p, s_i)$	$\checkmark, v_{ts}^{\lim}(V_D, s_i)$	
Rakha et al. (22)	$P_e^{FL}(v_i, \varphi_g)$	\checkmark	\checkmark, w_{gb}	\checkmark, t_{db}	\times	\times	
Fadhloun et al. (23)	\times, P_e^{\max}	\checkmark	\times	$\checkmark, t_{db}(v_i, V_D)$	\times	\times	
Fadhloun et al. (6)	$\times, \beta(v_i) \cdot P_e^{\max}$	\checkmark	\times	$\checkmark, w_{db}(v_i, v_i^p, V_D, s_i)$			
Makridis et al. (7) - MFC	$P_e^{FL}(v_i, \varphi_g)$	\checkmark	$\checkmark, w_{gb}(GS)$	$\checkmark, w_{db}(v_i, V_D, DS)$	\times	\times	

Note: β = the full-load engine power adjustment factor; V_D = the desired speed or roadway free-flow speed; v_i^p = the speed of the preceding vehicle; s_i = the vehicle spacing from the front bumper of the subject vehicle to the back bumper of the preceding vehicle; GS and DS = calibratable parameters capturing different drivers' gearshift style and driving style, respectively; MFC = microsimulation free-flow acceleration model.

^aThe full-load engine power (P_e^{FL}) across the entire operating speed range can be expressed as:

- (i) P_e^{\max} , which is a constant and equal to the peak power that the engine can produce; or
- (ii) $\beta(v_i) \cdot P_e^{\max}$, which is a percentage of the peak engine power; or
- (iii) $P_e^{FL}(v_i, \varphi_g)$, which is a function of the vehicle speed v_i and the engaged gear ratio φ_g .

^bThe gear shifting points within the vehicle speed range are defined by w_{gb} for each driver.

^cThe driver's typical driving pattern can be represented as a percentage of the vehicle's full-load capabilities in two methods:

- (i) multiplying the full-load engine power curve by a power reduction (or throttle opening) factor, t_{db} ; and
- (ii) multiplying the vehicle acceleration potential curve by an acceleration reduction factor, w_{db} .

Both of the above factors can be a constant or a function (symbols with arguments in parentheses) for each driver.

^dThe terms of collision avoidance and traffic stability belong to the vehicle interaction branch in car-following models, as mentioned above. They can be either expressed as speed limit functions (i.e., v_{ca}^{\lim} and v_{ts}^{\lim} , respectively) or directly incorporated into the driving behavior function w_{db} .

desired speed V_D . In 2019 Fadhloun et al. (6) further improved the model by incorporating the two vehicle interaction constraints (i.e., collision avoidance and steady-state traffic stream) into the driving behavior function $w_{db}(v_i, v_i^p, V_D, s_i)$ which acted as an acceleration reduction factor. Makridis et al. (7) demonstrated the first study to account for different drivers' driving behavior and gearshift behavior simultaneously, by introducing two calibratable parameters, namely, driving style (DS) and gearshift style (GS).

None of the studies reviewed so far, however, accounted for the acceleration dynamics of the electrified vehicle, which has significantly different power characteristics from those of the conventional ICEV (8, 24) and is representative of an emerging trend in sustainable

transportation (25, 26). Furthermore, previous studies have not explicitly dealt with the vehicle's deceleration characteristics. The present research builds on the MFC free-flow acceleration model (7) and proposes an extension to introduce the dynamics of electrified vehicles for free-flow microsimulation modeling. The enhanced model is extensively tested in the following dimensions:

- Validation of acceleration and deceleration potential curves underlying the MFC model, using laboratory chassis dynamometer tests of an electrified vehicle.
- Implementation of the MFC model in microsimulation with various acceleration and deceleration scenarios.

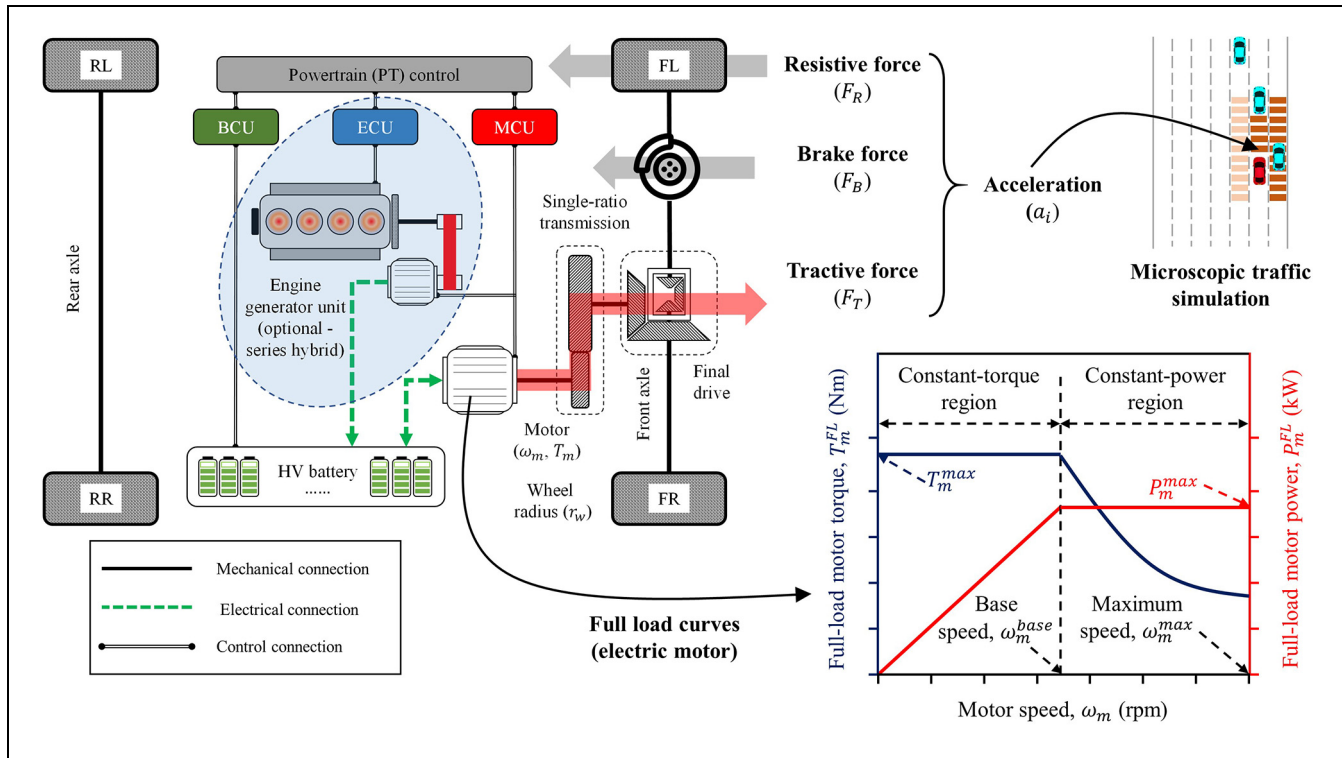


Figure 1. Introducing the dynamics of the electrified vehicle into microsimulation.

Note: RL = rear-left wheel; RR = rear-right wheel; FL = front-left wheel; FR = front-right wheel; BCU = battery control unit; ECU = engine control unit; MCU = motor control unit; HV = high-voltage.

- Calibration and validation of the MFC, Gipps, and IDM models using on-road driving trajectories.
- Validation based on the official 0–100 km/h acceleration time from the vehicle specification database that contains information relating to 59 commercial electrified vehicles.

This paper is organized as follows. First, a comprehensive description of the proposed model is presented. The following section then describes the experimental setup, which includes chassis dynamometer tests in the Vehicle Emissions Laboratories (VELA) of the European Commission, the on-road experimental campaign, the publicly available electrified vehicle specifications, and two behavioral models (Gipps and IDM) that are used in the validation workflow for comparison purposes. Afterward, the results are presented and the final section discusses the conclusions as well as future work.

Description of the Enhanced MFC Model

To the best of the authors' knowledge, the enhanced MFC model proposed in this study is so far the only free-flow model that incorporates the electrified vehicle's power and deceleration dynamics. It has three key functional components: the acceleration potential (a_{ap}) curve,

the deceleration potential (a_{dp}) curve, and the driving behavior (w_{db}) function. The logic behind them is straightforward to understand. The model computes the vehicle's theoretical capabilities, namely, a_{ap} and a_{dp} curves, according to its official specifications and chassis dynamometer tests. The percentage of these capabilities that drivers typically use is then formulated as the driving behavior function w_{db} .

The model presented in this study is applicable to the battery (or pure) electric and series hybrid electric vehicles (i.e., BEVs and series-HEVs). However, the same principles can be used to simulate any electrified vehicle. After all, the underlying MFC methodology was designed to offer as broad vehicle coverage as possible. As shown in Figure 1 (left), BEVs and series-HEVs are directly driven by electric motor, and adopt the single-ratio transmission gearbox because the motor has a larger operating speed range than that of the internal combustion engine, thus, no gear shift effects are involved. It is worth noting that, in a series-HEV, instead of driving the wheels, the internal combustion engine merely acts as an onboard charging component. The more advanced MFC model for complex hybrid configurations, for example, power-split (27), involving speed and torque coupling between the electric motor and the internal combustion engine, are still under development and will not be discussed in this paper. The examined

vehicles adopt single-ratio transmission, as mentioned above, so the gearshifting functionality of the MFC model was not elaborated further in the present study.

Acceleration Potential Curve

The acceleration potential (a_{ap}) curve captures the maximum acceleration across the entire vehicle speed range and varies as a function of the vehicle speed, as described in Equation 1.

$$\begin{cases} a_{ap}(v_i) = \frac{F_T^{FL}(v_i) - F_R(v_i)}{m}, \\ F_T^{FL}(v_i) = \min\left(\frac{T_T^{FL}(v_i)}{r_w}, \mu \cdot m_{ta} \cdot g\right), \end{cases} \quad (1)$$

where v_i is the current vehicle speed (m/s); m is the vehicle operating mass (kg); r_w is the wheel radius (m); F_R is the total resistance force (N), including the aerodynamics, the rolling and the grade resistances; μ is the coefficient of friction between wheels and roadway surface; m_{ta} is the mass of the vehicle on the tractive axle (kg); g is the gravitational acceleration (m/s²); F_T^{FL} and T_T^{FL} respectively denote the vehicle's tractive force (N) and tractive torque (Nm) at full-load conditions. As mentioned in the previous paragraphs, a single-ratio transmission gearbox is adopted, thus, T_T^{FL} can be directly derived from the full-load characteristics of the electric motor.

$$T_T^{FL}(v_i) = T_m^{FL}(\omega_m) \cdot \varphi_g \cdot \eta_d, \quad (2)$$

$$\omega_m(v_i) = \frac{60 \cdot \varphi_g \cdot v_i(t)}{2\pi \cdot r_w}, \quad (3)$$

where ω_m and T_m^{FL} are the rotational speed (rpm) of the electric motor, and the maximum achievable (full-load) motor torque (Nm) at this speed, respectively; φ_g is the fixed gear ratio of the transmission gearbox; and η_d is driveline efficiency. Equation 3 presents the relation between the vehicle longitudinal motion speed v_i and the motor rotational speed ω_m .

Figure 1 (bottom right) qualitatively explains the speed-torque-power characteristics of the normal electric motor (28) at full-load conditions. From this graph, two distinct motor operation regions are observed. First, in the lower speed region ($\omega_m < \omega_m^{\text{base}}$) or the constant-torque region, the full-load motor torque T_m^{FL} is constant and equal to the motor's peak torque T_m^{max} ; however, the full-load motor power P_m^{FL} is directly proportional to the motor speed. Second, in the higher speed region or the constant-power region, P_m^{FL} is constant and equal to the motor's peak power P_m^{max} , but T_m^{FL} varies as a reciprocal function of the motor speed. Accordingly, the motor's full-load torque T_m^{FL} can be described as a stepwise function of its rotational speed ω_m .

$$T_m^{FL}(\omega_m) = \begin{cases} T_m^{\text{max}}, & 0 \leq \omega_m(t) < \omega_m^{\text{base}} \\ \frac{6 \times 10^4 \cdot P_m^{\text{max}}}{2\pi \cdot \omega_m(t)}, & \omega_m^{\text{base}} \leq \omega_m(t) < \omega_m^{\text{max}} \end{cases} \quad (4)$$

where T_m^{max} and P_m^{max} are the motor's peak torque (Nm) and peak power (kW), respectively; ω_m^{max} is the motor's maximum permissible speed (rpm); ω_m^{base} is the motor base speed (rpm), representing the split point between constant-torque and constant-power regions, which can be calculated as Equation 5.

$$\omega_m^{\text{base}} = \frac{6 \times 10^4 \cdot P_m^{\text{max}}}{2\pi \cdot T_m^{\text{max}}}, \quad (5)$$

The model also computes the variable resistance force F_R that acts on the vehicle, as demonstrated in Equation 6.

$$F_R(v_i) = f_0 \cdot \cos(\theta) + f_1 \cdot v_i + f_2 \cdot v_i^2 + mg \cdot \sin(\theta), \quad (6)$$

where θ is the road grade; f_0 , f_1 , and f_2 are road load coefficients. A dedicated method for the calculation of the vehicle's road load coefficients presented by Tsiakmakis et al. (29) is adopted in this work.

Deceleration Potential Curve

It is important to stress that the deceleration potential (a_{dp}) curve is an essential upgrade for the MFC model (7) and marks a first attempt to incorporate the vehicle's deceleration characteristics explicitly in car-following models. According to Fadhloun et al. (6), the vehicle's deceleration capability has to be bound by the deceleration limit a_d^{lim} (namely, the product of the gravitational acceleration g and the road friction coefficient μ), as expressed in Equation 7.

$$a_d^{\text{lim}} = \mu \cdot g, \quad (7)$$

Besides the theoretical capability, the a_{dp} curve should account for the deceleration rates that are acceptable to drivers in the field. A reasonable approach to tackle this issue could be to introduce a reduction factor ξ that varies as a function of the vehicle speed v_i , as given in Equation 8. The factor ξ utilizes a quadratic functional form proposed and validated by Akhilesh et al. (30) for typical passenger cars examined in this paper.

$$a_{dp}(v_i) = \xi(v_i) \cdot a_d^{\text{lim}}, \quad (8)$$

$$\xi(v_i) = d_2 \cdot v_i^2 + d_1 \cdot v_i + d_0, \quad (9)$$

where the theoretical deceleration limit a_d^{lim} is assumed to be constant and equal to 7.72 m/s² in this study; d_0 , d_1 , and d_2 are coefficients equal to -0.2439, -0.0221, and 0.0006, respectively, based on the data from chassis

Table 2. Variables and Parameters of the Enhanced MFC Model

	Acceleration potential (a_{ap}) curve	Deceleration potential (a_{dp}) curve	Driving behavior function (w_{db})
Equations	1–6	7–9	10–11
State variables	a_i, v_i, t, θ		
Available in or determined by publicly available specifications	$F_T^{FL}(v_i), F_R(v_i), T_T^{FL}(v_i), T_m^{FL}(\omega_m), \omega_m(v_i); m, g, \mu, m_{ta}, r_w, \varphi_g, \eta_d, T_m^{\max}, P_m^{\max}, \omega_m^{\text{base}}, \omega_m^{\max}, f_0, f_1, f_2$	a_d^{\lim}	na
Determined by chassis dynamometer tests	na	$\xi(v_i); d_0, d_1, d_2$	na
From microsimulation	na	na	$V_D(t); c_0, c_1, c_2, c_3$
Determined by model calibration	na	na	DS

Note: na = not applicable; MFC = microsimulation free-flow acceleration model. Main symbols: F = force; T = torque; P = power; a = acceleration; v = velocity; ω = rotational speed; t = time; θ = road grade; m = mass; g = gravitational acceleration; μ = coefficient of friction; f , d , and c = constant coefficients; DS = driving style; ξ = reduction factor. Main subscripts: i = current instance; T = tractive; R = resistance; ta = tractive axle; m = motor; ap = acceleration potential; dp = deceleration potential; db = driving behavior. Main superscripts: FL = full-load; \max = maximum; \lim = limit; $base$ = base. Other variables or parameters: r_w = wheel radius; φ_g = gear ratio; η_d = driveline efficiency; V_D = desired (or roadway free-flow) speed; a_d^{\lim} = deceleration limit.

dynamometer deceleration tests, which ensure that vehicle decelerations are realistic.

Driving Behavior Function

To make the model representative of different driving patterns, the driving behavior function is incorporated as a variable reduction factor multiplied by a_{ap} and a_{dp} curves. The resulting formula, as demonstrated in Equation 10, allows modeling of the typical acceleration and deceleration behaviors that follow different driver characteristics.

$$a_i(t) = \begin{cases} w_{db}(v_i(t)) \cdot a_{ap}(v_i(t)), & 0 \leq \frac{v_i(t)}{V_D(t)} < 1 \\ w_{db}(v_i(t)) \cdot a_{dp}(v_i(t)), & \frac{v_i(t)}{V_D(t)} \geq 1 \end{cases} \quad (10)$$

where V_D is the desired (or roadway free-flow) speed (m/s); w_{db} is the driving behavior function, whose expression is given below.

$$w_{db}(v_i(t)) = \begin{cases} DS \cdot \left(1 - c_1 \cdot \left(1 - \frac{v_i(t)}{V_D(t)}\right)^{c_0}\right), & 0 \leq \frac{v_i(t)}{V_D(t)} < 0.5 \\ DS \cdot \left(1 - \left(1 + \frac{v_i(t) - V_D(t)}{c_3}\right)^{c_2}\right), & 0.5 \leq \frac{v_i(t)}{V_D(t)} < 1 \\ DS \cdot \left(1 - \left(1 - \frac{v_i(t) - V_D(t)}{c_3}\right)^{c_2}\right), & \frac{v_i(t)}{V_D(t)} \geq 1 \end{cases} \quad (11)$$

where the factor DS represents the driving style and ranges between 0 and 1; the coefficients c_0 , c_1 , c_2 , and c_3 determine the way in which drivers approach the desired speed and are set as 60, 0.8, 100, and 50, respectively. What is important to recognize here is that the driving behavior function is different from that of the original MFC model (7), to incorporate the deceleration potential curve and offer a much smoother acceleration profile.

Table 2 summarizes all the variables and parameters in the enhanced MFC model, categorizes them into different groups according to their sources, and explains their main symbols, subscripts, and superscripts. Most of the elements involved in this model are derived directly from the publicly available specifications, the data in chassis dynamometer tests, and the predefined microsimulation scenarios. Table 2 highlights that the proposed model requires the calibration of only one parameter, namely, driving style (DS), completely ruling out the effect of the number of calibration parameters on any potential increase in model complexity.

To conclude this section, the enhanced MFC model presented here is hitherto the only investigation to incorporate the dynamics of electrified vehicles into microsimulation. The following equations and corresponding parameters highlight the original and important contributions of this study to the field of dynamics-based car-following models. First, the electric motor's full-load torque and power characteristics are captured by Equations 2–5 using publicly available specifications. Second, in the chassis dynamometer tests, the observed deceleration

Table 3. Main Specifications of the Electrified Vehicle under Test

Specifications	Symbols	Units	Values
Vehicle operating mass	<i>m</i>	kg	1420
Motor's peak torque	T_m^{\max}	Nm	295
Motor's peak power	P_m^{\max}	kW	88
Single-speed gear ratio	φ_g	na	7.412
Wheel radius	r_w	m	0.316
Vehicle speed limit	v_{\lim}	km/h	165
Height	<i>H</i>	m	1.45
Width	<i>W</i>	m	1.82
0–100 km/h acceleration time	$T_{0-100\text{km/h}}$	s	9.9

Note: na = not applicable.

capability of the electrified vehicle is fitted by a quadratic function as shown in Equations 7–9. Finally, the newly developed driving behavior function in Equations 10 and 11 provides a bridge connecting the vehicle's acceleration and deceleration potential curves.

Experimental Setup

This section describes the experimental setup, which includes chassis dynamometer tests in the VELA laboratory, the on-road experimental campaign, the publicly available electrified vehicle specifications, and two behavioral models (Gipps and IDM) that are used in the validation workflow for comparison purposes.

Validation using VELA Data

To validate the reliability of the acceleration and deceleration potential curves (i.e., a_{ap} and a_{dp}), chassis dynamometer tests were carried out at the VELA Joint Research Centre (JRC). A 2016 Hyundai Ioniq electric vehicle, whose main specifications are listed in Table 3, was selected to conduct 46 consecutive acceleration–deceleration test cycles. More specifically, the vehicle was tested within a speed range between 20 and 120 km/h, in relation to three different drive modes (i.e., normal, eco, and sport), three different pedal positions (i.e., mild, normal, and full), and four levels of regenerative braking. The testbed can collect data with a 10 Hz measurement rate.

Calibration and Validation using On-Road Data

Figure 2 illustrates the on-road campaign carried out in typical highway driving scenarios. Therefore, unusual circumstances such as traffic crashes and congestions are not considered. Field tests were conducted on a section of Autostrada A26 (Italy) between Vicolungo and Ghemme, a 32 km round trip, to collect driving data under real-world traffic conditions for the model calibration and validation. The test vehicle was equipped with a

multi-constellation global navigation satellite system (GNSS) receiver, able to collect GNSS data with a 10 Hz measurement rate. The horizontal accuracy reported by the receiver is less than 50 cm. The GNSS active antenna was mounted on the roof of the vehicle, to ensure maximum satellite visibility and avoid signal attenuation from the vehicle body. At each time instant, the geographic coordinates (latitude, longitude, and altitude) of the vehicle were recorded, which were then transformed into a local east, north, and up (ENU) Cartesian reference frame. The outliers were filtered using typical moving average post-processing. The test section comprises various uphill and downhill segments, providing an appropriate environment to examine different tractive load conditions. The elevation profile of the test route is extracted using GPS Visualizer. The road grade varies approximately between -8% and 8%.

Figure 2, *a* and *b*, show the northbound (Cycle I) and southbound (Cycle II) driving profiles, respectively, where the speed varies between 10 and 40 m/s and the acceleration ranges from -4 to 2 m/s². The MFC model is calibrated and validated, using Cycle I and II, respectively, against the other two widely used behavioral models (Gipps and IDM), whose expressions will be subsequently introduced. Figure 2*c* demonstrates the model calibration and validation procedures. The model parameters are calibrated using the on-road data (Cycle I) and the LMFIT (non-linear least-squares minimization and curve-fitting) optimization tool. After determining the optimal parameters, the models are then tested using Cycle II to further validate the models' robustness and reliability. According to the method discussed in the work of Treiber and Kesting (31), the calibration objective function is defined based on the sums of squared errors, as described in Equation 12.

$$V^{\text{rel}}(M_{\hat{x}}) = \sum_{j=1}^n \left(\ln \left(\frac{v_{M_{\hat{x}}}(j)}{v_N(j)} \right) \right)^2, \forall M, \hat{x} \quad (12)$$

where *j* is a distance instance (every 2 m along the predefined path); v_N is the measured speed from the naturalistic on-road driving; $v_{M_{\hat{x}}}$ is the simulated speed by the model *M* with a parameter vector \hat{x} . The calibration parameters and their constraints are shown in Table 4.

Validation using 0–100 km/h Acceleration Specifications

A vehicle specification dataset developed by JRC contains information relating to 59 commercial electrified vehicles. Figure 3 exhibits the main specifications associated with their acceleration performances, including the power, torque, and speed limits of the electric motor, the vehicle mass, the wheel radius, and the

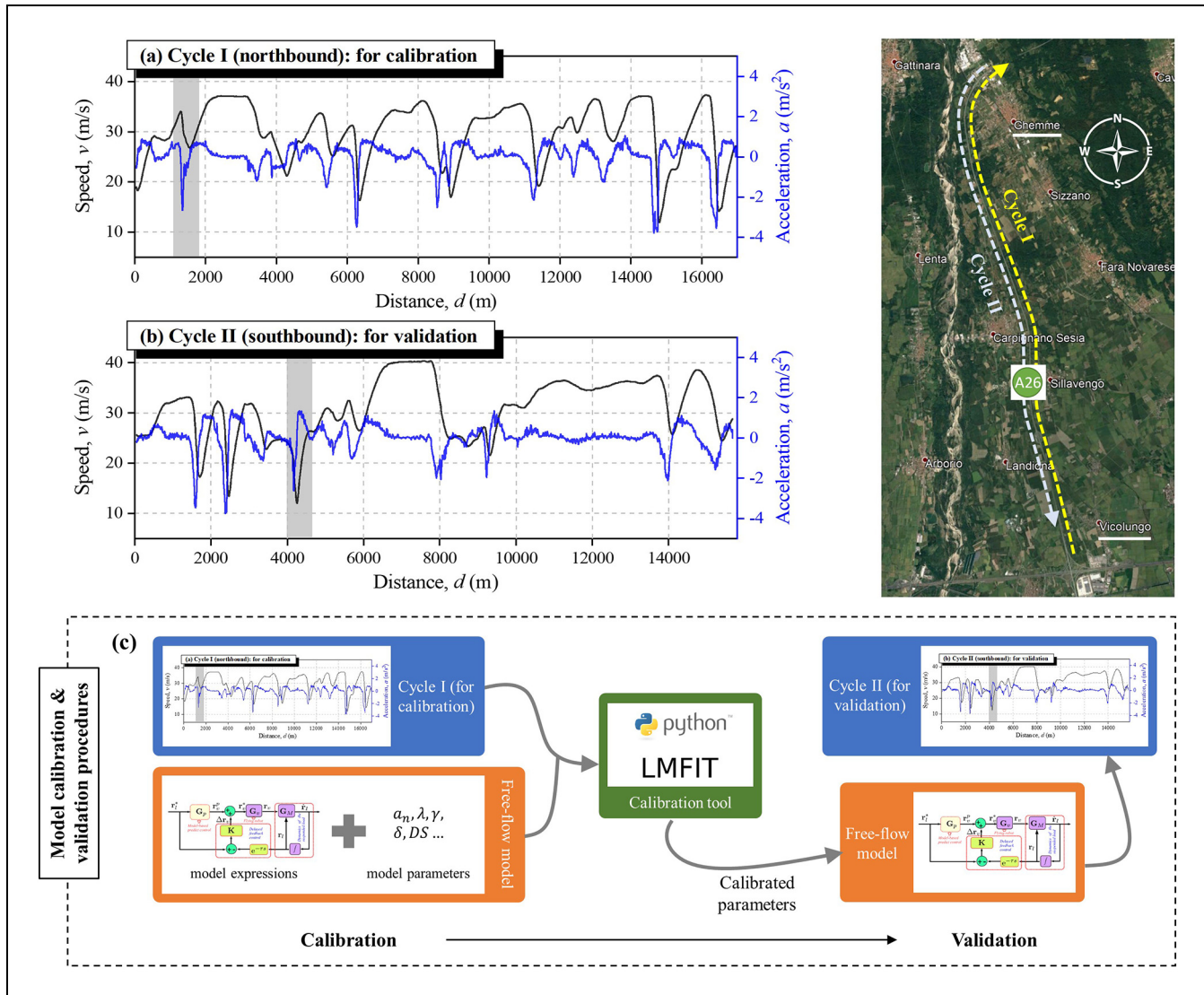


Figure 2. On-road driving campaign for model calibration and validation: (a) northbound (Cycle I) and (b) southbound (Cycle II) driving profiles; and (c) model calibration and validation procedures.

Table 4. Calibration Parameters and Their Constraints

Model	Parameters
Gipps	$a_n \in [0.5, 4]$, $\lambda \in [0.001, 5]$, $\gamma \in [0.5, 4]$
IDM	$a_n \in [0.5, 4]$, $\delta \in [0.1, 4]$
MFC	$DS \in [0.1, 1]$

Note: IDM = intelligent driver model; MFC = microsimulation free-flow acceleration model.

transmission gear ratio. What is interesting about the data in this parallel plot is that positive correlations can be found among P_m^{\max} , T_m^{\max} , ω_m^{\max} , and m , suggesting that stronger performances of the electric motor are usually associated with a larger vehicle mass. Furthermore, better motor performances (i.e., P_m^{\max} , T_m^{\max} , and ω_m^{\max}) can

significantly reduce the 0–100 km/h acceleration time ($T_{0-100\text{km}/\text{h}}$), whose value ranges from 2.7 to 14.5 s in this dataset.

Benchmark Models

The enhanced MFC model is validated against another two state-of-the-art behavioral models: Gipps and IDM. The expression of the Gipps model's free-flow branch is given below.

$$a_i(t) = \max \left(\alpha \cdot a_n \cdot \left(1 - \frac{v_i(t)}{V_D} \right) \cdot \left(\lambda + \frac{v_i(t)}{V_D} \right)^\gamma, b_n \right), \quad (13)$$

where v_i (m/s) and a_i (m/s²) are the state variables at time t (s); V_D is the desired speed (m/s); a_n is the desired

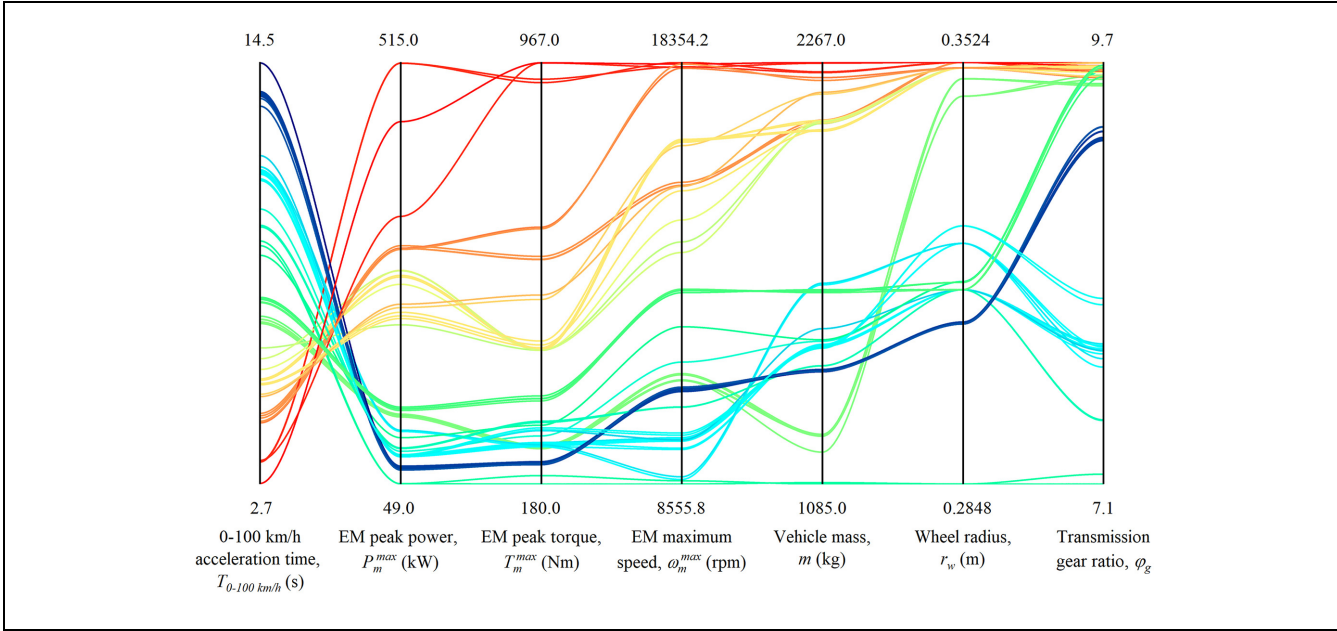


Figure 3. Main specifications of 59 electrified vehicles from the dataset.

Note: EM = electric motor.

acceleration (m/s^2); and b_n indicates the vehicle's maximum deceleration rate and is equal to -3 m/s^2 . Ciuffo et al. (32) reported that the constant parameters, α , λ , and γ in Gipps model have the following relationship.

$$\alpha = \frac{(1 + \gamma)^{1 + \gamma}}{\gamma^\gamma \cdot (1 + \lambda)^{1 + \gamma}}, \quad (14)$$

IDM is another benchmark model, whose free-flow driving behavior is similar to the work conducted by Schakel et al. (33) using the following expression.

$$a_i(t) = \max\left(a_n \cdot \left(1 - \frac{v_i(t)}{V_D}\right)^\delta, b_n\right), \quad (15)$$

where δ is a constant parameter. It is important to stress that many dynamics-based models in Table 1 are claimed to outperform the above benchmark models (i.e., Gipps and IDM) in generating realistic vehicle trajectories (34), but all of them are developed for conventional ICEVs. It is therefore time-consuming to adapt these models for electrified vehicles and recalibrate their parameters. Moreover, these dynamics-based models are often not widely implemented or extensively validated in commercial microscopic simulation software (e.g., AIMSUN, VISSIM, and PARAMICS). Therefore, in this paper, the proposed MFC model is not benchmarked against these dynamics-based models, which, however, can be considered in the authors' future studies.

Results and Discussion

This section presents a critical analysis of the results from the experimental and simulation tests described above.

Validation using VELA Data

Figure 4 displays the validation of the vehicle's acceleration and deceleration potential curves in the MFC model, using the data recorded during chassis dynamometer testing in the VELA laboratory. Figure 4a reports the 46 consecutive acceleration-deceleration test cycles that the vehicle performed. From the results achieved, Figure 4b compares the observed data points with the a_{ap} and a_{dp} curves resulting from the enhanced MFC model. It is worth noting that there are few test points in the low-speed (less than $\sim 5 \text{ m/s}$) region because the speed range for the acceleration test is between 20 and 120 km/h. The theoretical a_{ap} curve, derived directly from vehicle specifications, demonstrates a good correlation with the upper boundary test points. Besides, the empirical a_{dp} curve is very close to the lower boundary test points. Figure 4c selects the test points, whose acceleration rates are close to zero (namely, $a_i \in [-0.1, 0.1]$). In this condition, therefore, the tractive power P_T (kW) is approximately equal to the resistance power P_R (kW). The observed correlation between the theoretical P_R curve and measured P_T points can provide further support for the reliability of the MFC model.

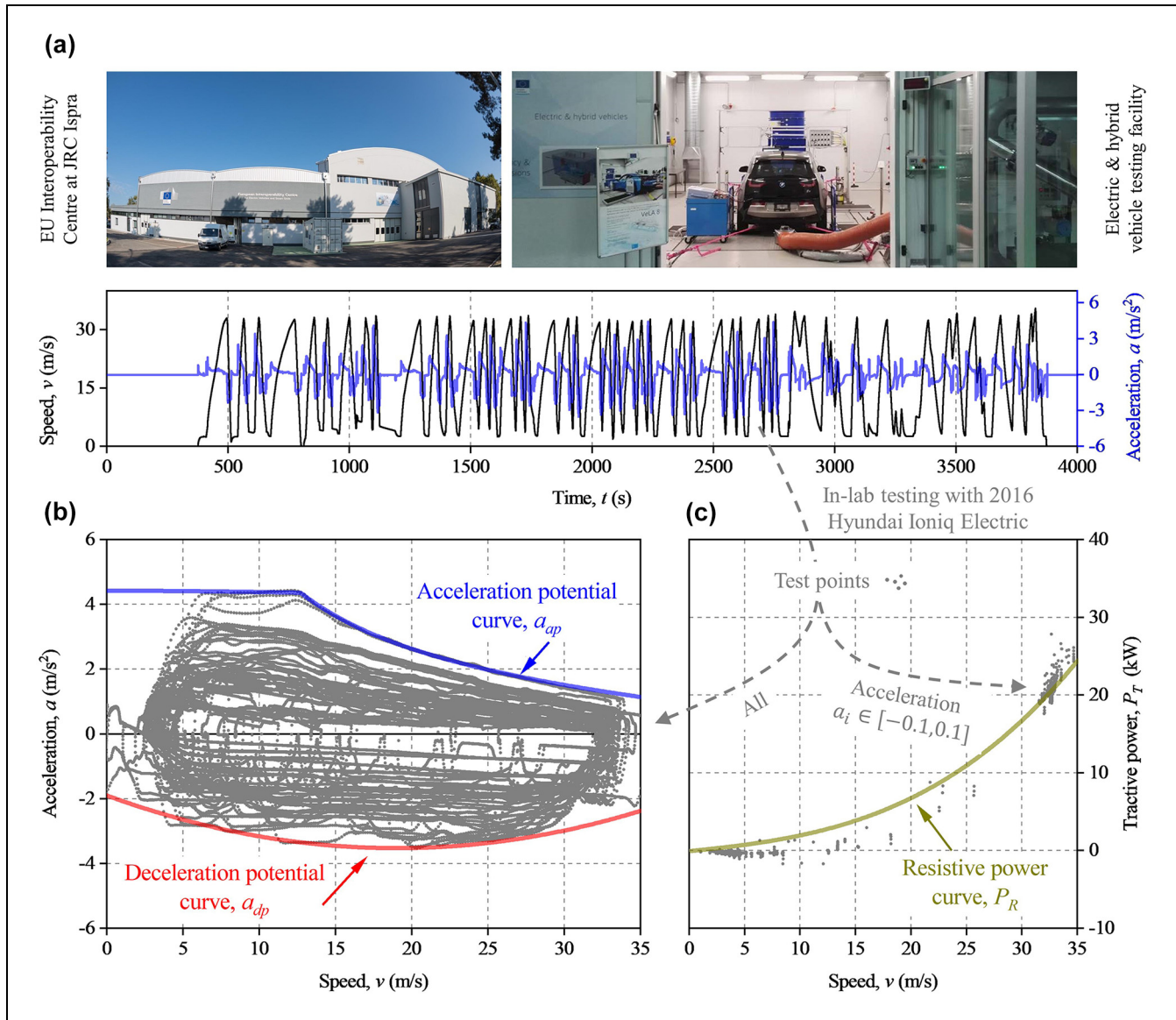


Figure 4. Chassis dynamometer tests of an electrified vehicle for the model validation: (a) testing facilities and driving profiles; (b) the validation of the acceleration and deceleration potential curves; and (c) the validation of the vehicle's theoretical resistive power.
Note: EU = European Union; JRC = Joint Research Centre.

Model Implementation in Microsimulation

Figure 5 presents the implementation of the enhanced MFC model in microsimulation, where changes in driving style factor DS (in driving behavior function w_{db}) are compared. Three indicative driving styles are selected for the same vehicle: (i) $DS = 1$, the most aggressive driver who utilizes the full acceleration and deceleration potentials when possible; (ii) $DS = 0.8$, the more timid one; and (iii) $DS = 0.6$, the most conservative driver.

Figure 5 provides the driving profiles of different drivers, during acceleration (from 0 to 45 m/s) (Figure 5, *a–c*) and deceleration (from 45 to 0 m/s) (Figure 5, *d–f*) scenarios. Moreover, Figure 5, *g–h*, show the results from

the driving simulation with varying road speed limits. What can be clearly seen in these plots is that the enhanced MFC model can ensure a smooth transition between different acceleration and deceleration levels while avoiding obvious oscillations or overshoots when approaching the reference speed. This smooth feature is praiseworthy given that significant and omnipresent acceleration cliffs are observed in many well-known car-following models (6). Additionally, the result is significant at point A in Figure 5*a* because it represents that the most aggressive driver ($DS = 1$) can accelerate from 0 to 100 km/h in 9.1 s, very close to the vehicle's specification ($T_{0-100\text{km/h}} = 9.9$ s) given in Table 3.

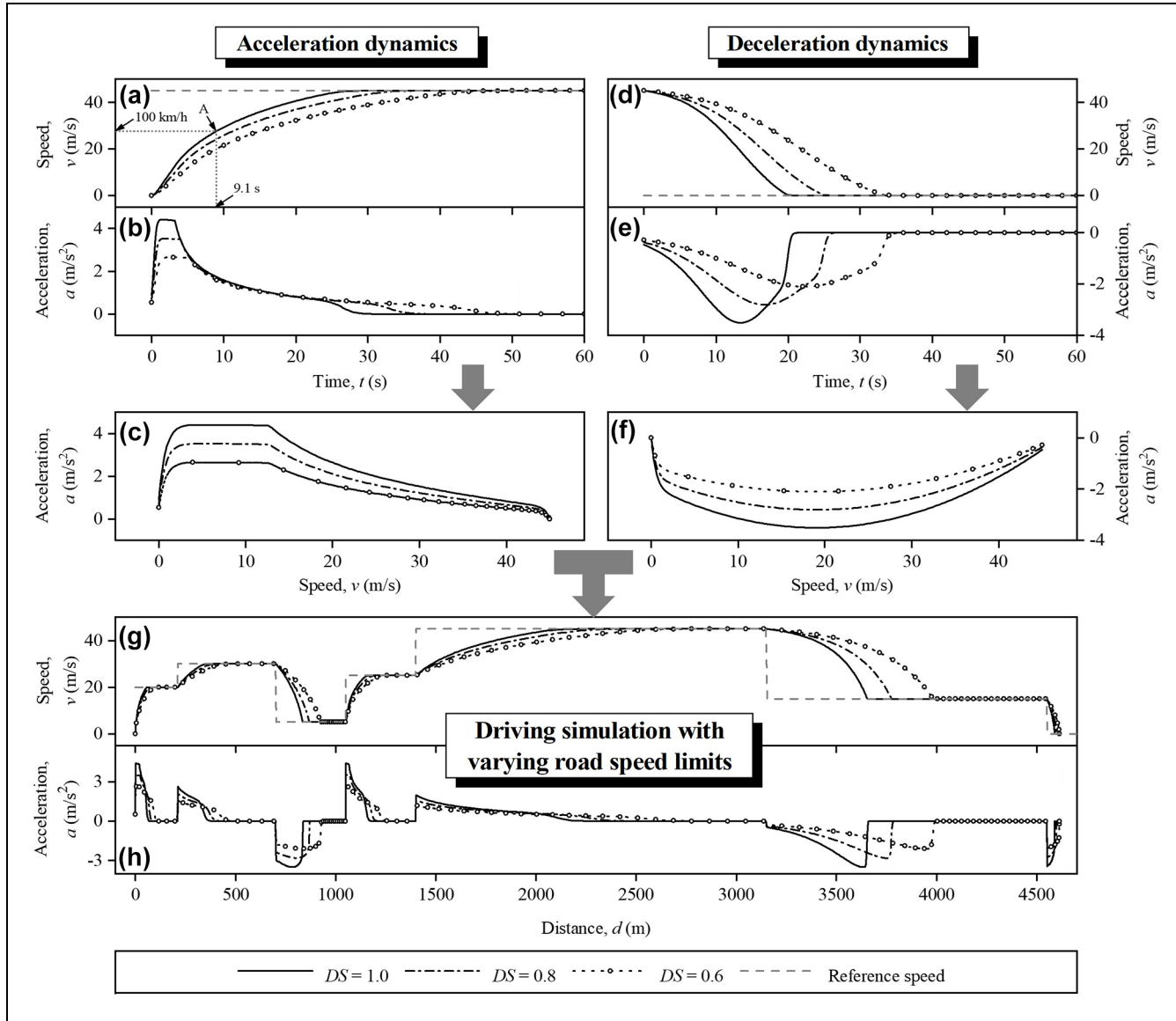


Figure 5. Implementation of the enhanced MFC model in microsimulation: (a) speed-time, (b) acceleration-time, and (c) acceleration-speed profiles in the vehicle acceleration scenario; (d-f) corresponding profiles in the vehicle deceleration scenario; and (g) speed-distance and (h) acceleration-distance profiles in driving simulation with varying road speed limits.

Note: MFC = microsimulation free-flow acceleration model; DS = driving style factor.

Calibration and Validation using On-Road Data

Figure 6, *a-d*, and Figure 6, *e-h*, show the statistical results from the model calibration and validation, respectively. Figure 6, *a* and *e*, compare the observed average speed \bar{v} from on-road driving and its corresponding predictions from three different models (MFC, Gipps, and IDM). Although small, the absolute percentage errors of these models in relation to average speed prediction are different, where the MFC model demonstrates the smallest prediction errors ($\sim 0.06\%$) and the best robustness. The RMSE (root mean square error) between the observed and predicted speed profiles are presented in

Figure 6, *b* and *f*. A clear benefit of the MFC model in the reduction of RMSE for speed could be identified in these graphs. For example, when tested with the validation cycle, the speed RMSE of the MFC model (0.37 m/s) is 68.8% and 68.5% lower than those of the Gipps model (1.18 m/s) and the IDM model (1.17 m/s), respectively.

From the perspective of acceleration profiles, Figure 6, *c* and *g*, compare on-road observations and corresponding model predictions, in relation to the average absolute acceleration $|\bar{a}|$. The MFC model leads to excellent $|\bar{a}|$ predictions, whose absolute percentage errors (0.30% and 0.50% in calibration and validation cycles,

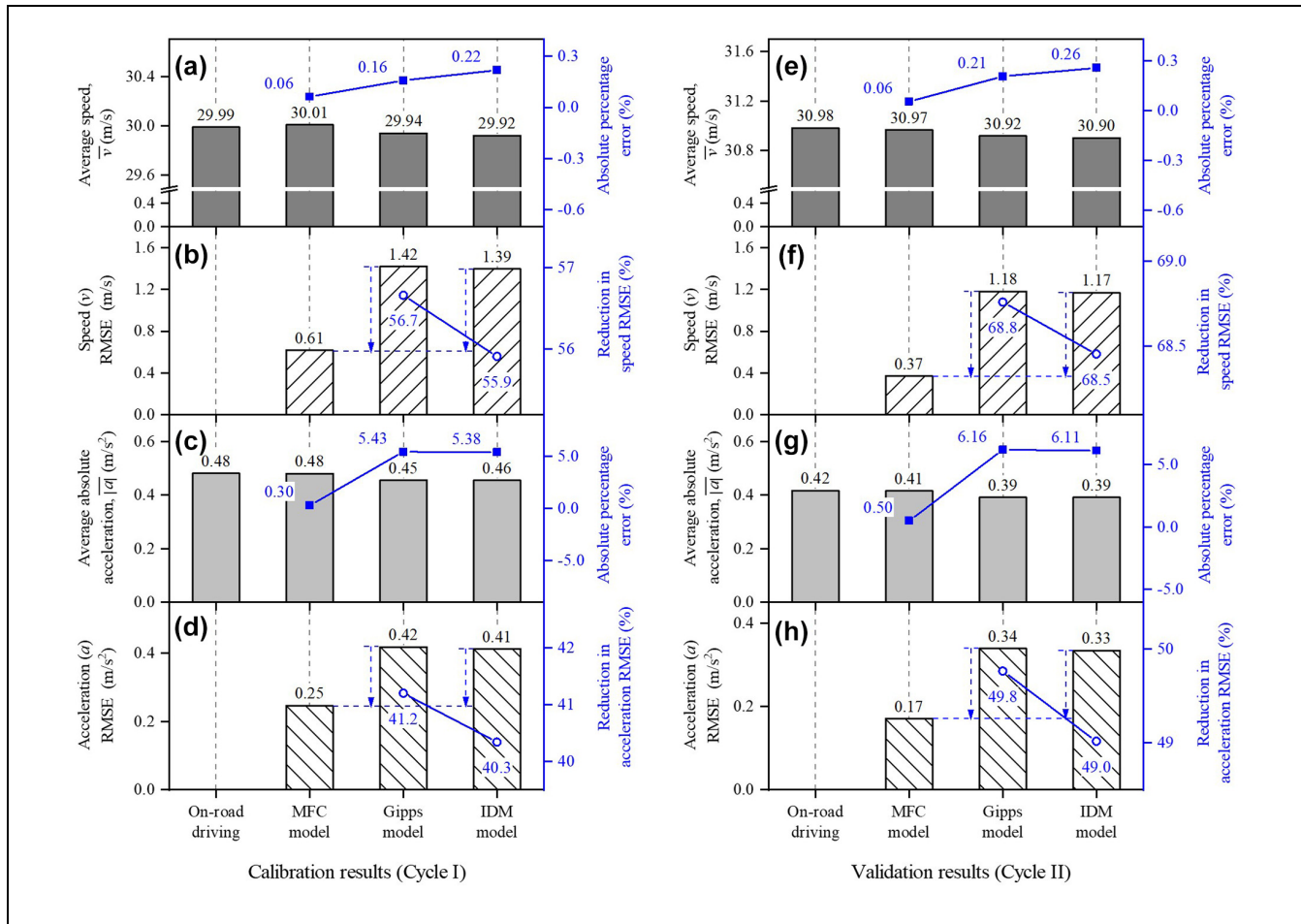


Figure 6. Statistical results of the model calibration and validation using on-road driving trajectories: (a) the error of the average speed, (b) the RMSE of speed, (c) the error of the average absolute acceleration, and (d) the RMSE of acceleration in model calibration; (e-h) corresponding results in model validation.

Note: MFC = microsimulation free-flow acceleration model; IDM = intelligent driver model; RMSE = root mean square error.

respectively) are an order of magnitude lower than those of the benchmark models. Figure 6, *d* and *h*, compare the RMSE of acceleration in different model predictions. The MFC model's advantage of accurately predicting the real acceleration behavior is demonstrated in these charts. In the validation test, for instance, the MFC model gives rise to an acceleration RMSE equal to 0.17 m/s^2 , which is 49.8% and 49.0% lower than those of benchmark models.

To offer a closer inspection of transient results, Figure 7 (left) and (right) present parts (the gray sections in Figure 2) of the distance–speed–acceleration profiles from calibration and validation cycles, respectively. As mentioned in the literature review, free-flow models regulate the subject vehicle by asymptotically approaching the desired speed V_D , such as MFC, Gipps, and IDM, as respectively defined in Equations 11, 13, and 15.

Consequently, a time delay exists between the speed prediction of the model and the desired speed (V_D). On the other hand, the driver's perception–response time delay in the free-flow driving experiments (illustrated in Figure 2) is not considered in this study. It is therefore assumed that the desired speed V_D is approximately the same as the driver's on-road driving speed for simplification purposes. This explains why time lags between the model predictions and the on-road trajectory are observed in Figure 7. As shown in these graphs, the three models appear successfully to produce a driving profile that emulates the on-road driving data. The Gipps and IDM models have very similar driving behaviors, and both introduce an obvious delay. However, the enhanced MFC model can capture both the speed and the acceleration dynamics much better. These results further support the findings in Figure 6.

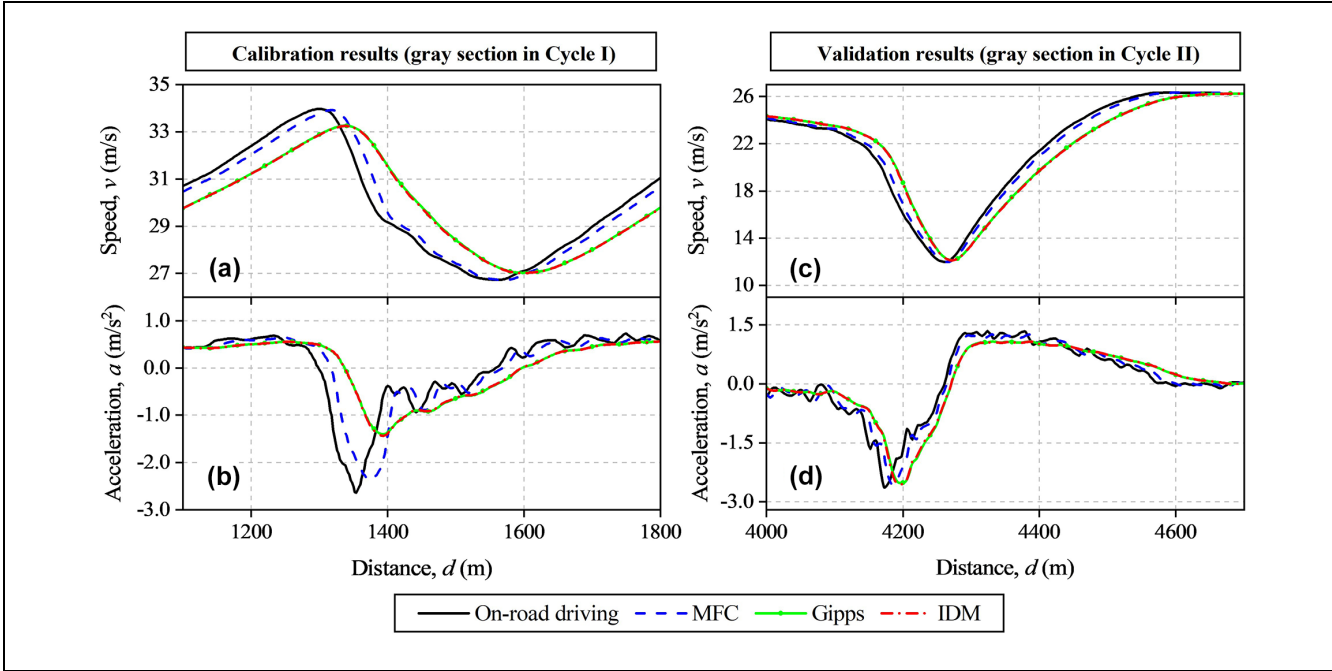


Figure 7. Transient results of the on-road observations and model predictions: (a and c) speed-distance profiles in the part of the Cycle I and Cycle II, respectively; (b and d) corresponding acceleration-distance profiles.

Note: MFC = microsimulation free-flow acceleration model; IDM = intelligent driver model.

Validation using 0–100 km/h Acceleration Specifications

In Figure 8, the models are further validated using vehicle acceleration specifications summarized in Figure 3, namely, 0–100 km/h acceleration time ($T_{0-100\text{km}/\text{h}}$). Figure 8a is a scatter plot of the acceleration time $T_{0-100\text{km}/\text{h}}^{\text{model}}$ from model predictions versus the acceleration time $T_{0-100\text{km}/\text{h}}^{\text{VS}}$ from the vehicle specification dataset, with varying marker color determined by the vehicle maximum power P_m^{max} . It can be seen that the cluster resulting from the MFC model is closely located around the diagonal, suggesting small errors between the predicted and specified values. On the other hand, as circled by the black boxes, Gipps and IDM models both significantly underestimate $T_{0-100\text{km}/\text{h}}$ values at the low P_m^{max} region. Furthermore, the Gipps model gives rise to overestimated predictions when P_m^{max} ranges from ~200 to ~300 kW.

Figure 8b shows the RMSE of the acceleration time $T_{0-100\text{km}/\text{h}}$ predicted by the three models. The benchmark models (Gipps and IDM) result in a $T_{0-100\text{km}/\text{h}}$ RMSE of 2.98 s and 3.49 s, respectively. Alternatively, the proposed MFC model can produce a much more accurate $T_{0-100\text{km}/\text{h}}$ prediction, whose RMSE is equal to 1.51 s and is 49.4% and 56.8% lower than those of Gipps and IDM, respectively. Figure 8c illustrates the distributions of the models' prediction errors. The peak in MFC distribution is higher and most of the sample points are

concentrated around zero, suggesting that the prediction error is significantly reduced.

Conclusion

This work builds on the MFC model and proposes an enhancement for the microsimulation of electrified vehicles, whose acceleration capability is different than that of traditional ICEVs. Furthermore, this paper develops an improved deceleration model to capture the deceleration capability of the vehicle at a given speed, which imposes realistic decelerations in microsimulation. The results of this study show that:

- The acceleration and deceleration potential curves underlying the enhanced MFC model can accurately represent the real dynamics of the electrified vehicle tested on the chassis dynamometer;
- In the microsimulation implementation, the enhanced MFC model can ensure a smooth transition between different acceleration and deceleration levels while avoiding obvious oscillations or overshoots when approaching the reference speed;
- When reproducing the on-road driving trajectories, the enhanced MFC model can deliver significant reductions in RMSE of speed (by ~69%) and acceleration (by ~50%) compared with benchmarks;

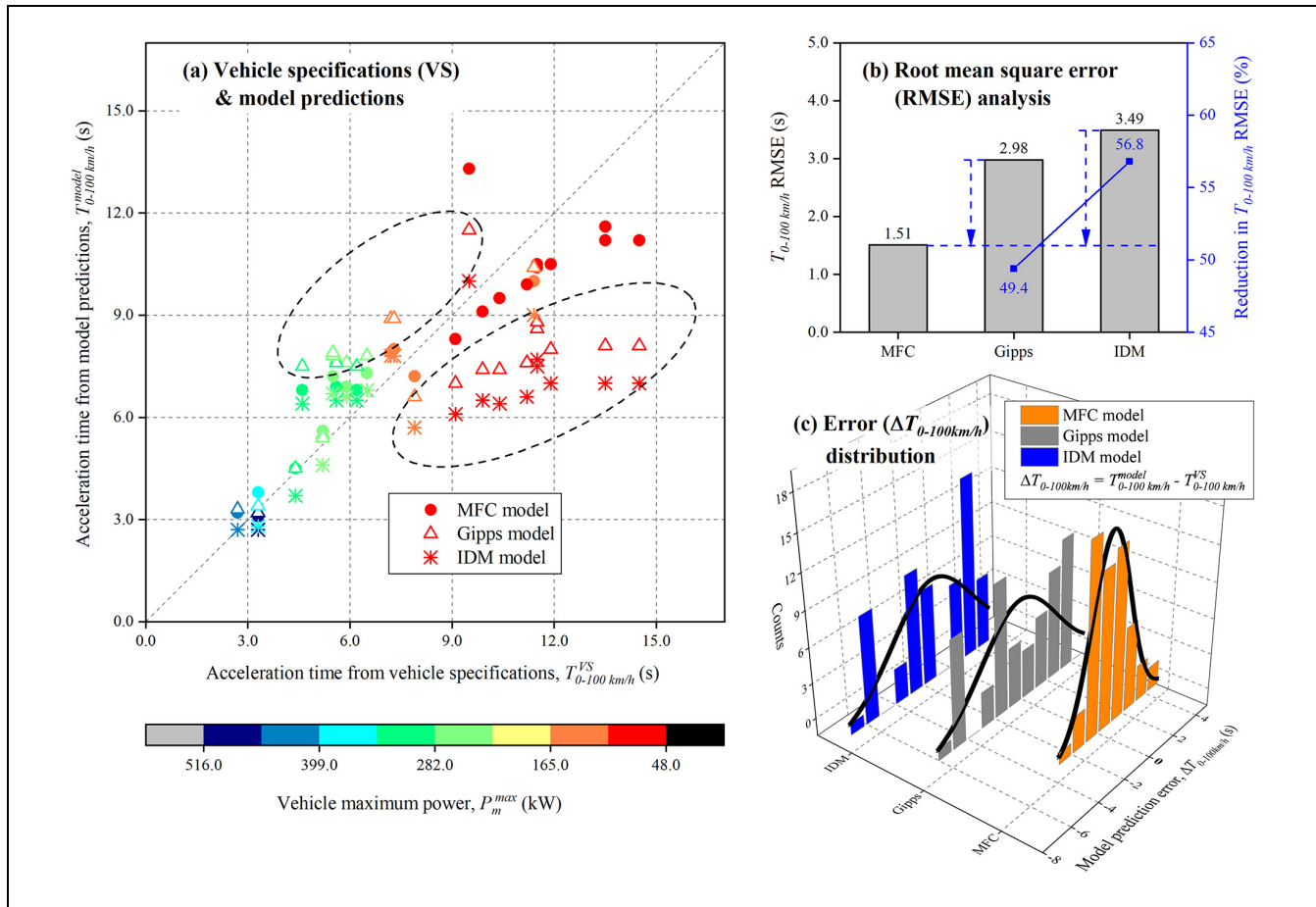


Figure 8. Validation using official 0–100 km/h acceleration specifications: (a) comparison of 0–100 km/h acceleration time between model predictions and vehicle specifications; (b) RMSE of 0–100 km/h acceleration time from model predictions; and (c) the distribution of models' prediction errors.

Note: MFC = microsimulation free-flow acceleration model; IDM = intelligent driver model.

- The enhanced MFC model can accurately predict the vehicle 0–100 km/h acceleration specifications, where its RMSE is 49.4% and 56.8% lower than those of Gipps and IDM models, respectively.

The study makes several contributions to the current literature:

- This paper provides the first comprehensive review and comparison of dynamics-based car-following (including free-flow) models;
- The enhanced MFC model is hitherto the only car-following model that accounts for acceleration dynamics of electrified vehicles;
- The enhanced MFC model marks a first attempt to incorporate explicitly the vehicle's deceleration characteristics in microsimulation.

However, to develop a more capable dynamics-based MFC model used in microsimulation, additional studies will be needed, as follows:

- The current deceleration potential curve is empirically derived from the data in chassis dynamometer tests, limiting its flexibility in the implementation of microsimulation. Therefore, it would be better if a theoretical method could be proposed;
- A more advanced MFC model is needed that can deal with the speed and torque coupling between the internal combustion engine and the electric motor in complex hybrid powertrain configurations;
- The proposed MFC model is validated in typical highway driving scenarios. However, unusual circumstances, such as traffic crashes and congestion, should also be considered when validating the model with regard to reproducing the empirical driver and vehicle behavior;
- The authors have started working on a project to couple the proposed dynamics-based car-following model (MFC) with their previously developed fuel

consumption and emission model (CO₂MPAS). The resulting open-source Python package has been published to PyPI (<https://pypi.org/project/co2mpas-driver/>). However, more effort is required to validate the performance of the MFC model extensively for predicting the vehicle's fuel consumption and emissions.

Acknowledgments

This work was based on a collaboration agreement between the Joint Research Centre of the European Commission and the University of Birmingham. The authors are grateful to Eleftherios-Nektarios Grylonakis and Vincenzo Arcidiacono, who contributed to the data processing, as well as to Fabrizio Minarini, Norbert Brinkhoff-Button, Daniele Borio, Alessandro Tansini, Aikaterini Anesiadou, and Melania Susi for their support during the experimental campaign.

Author Contributions

The authors confirm contributions to the paper as follows: study conception and design: Michail Makridis, Biagio Ciuffo, and Georgios Fontaras; data collection: Michail Makridis and Konstantinos Mattas; model development: Michail Makridis, Yinglong He, and Georgios Fontaras; analysis and interpretation of results: Michail Makridis, Georgios Fontaras, and Yinglong He; draft manuscript preparation: Yinglong He and Michail Makridis; model revision and comments: Michail Makridis and Georgios Fontaras. All authors reviewed the results and approved the final version of the manuscript.

Declaration of Conflicting Interests

The author(s) declared no potential conflicts of interest with respect to the research, authorship, and/or publication of this article.

Funding

The author(s) received no financial support for the research, authorship, and/or publication of this article.

References

- Pavlovic, J., B. Ciuffo, G. Fontaras, V. Valverde, and A. Marotta. How Much Difference in Type-Approval CO₂ Emissions from Passenger Cars in Europe Can Be Expected from Changing to the New Test Procedure (NEDC vs. WLTP)? *Transportation Research Part A: Policy and Practice*, Vol. 111, 2018, pp. 136–147.
- Fontaras, G., B. Ciuffo, N. Zacharof, S. Tsakmakis, A. Marotta, J. Pavlovic, and K. Anagnostopoulos. The Difference between Reported and Real-World CO₂ Emissions: How Much Improvement Can Be Expected by WLTP Introduction? *Transportation Research Procedia*, Vol. 25, 2017, pp. 3933–3943.
- He, Y., Q. Zhou, M. Makridis, K. Mattas, J. Li, H. Williams, and H. Xu. Multiobjective Co-Optimization of Cooperative Adaptive Cruise Control and Energy Management Strategy for PHEVs. *IEEE Transactions on Transportation Electrification*, Vol. 6, No. 1, 2020, pp. 346–355.
- He, Y., M. Makridis, G. Fontaras, K. Mattas, H. Xu, and B. Ciuffo. The Energy Impact of Adaptive Cruise Control in Real-World Highway Multiple-Car-Following Scenarios. *European Transport Research Review*, Vol. 12, 2020, pp. 1–11.
- Ciuffo, B., M. Makridis, T. Toledo, and G. Fontaras. Capability of Current Car-Following Models to Reproduce Vehicle Free-Flow Acceleration Dynamics. *IEEE Transactions on Intelligent Transportation Systems*, Vol. 19, No. 11, 2018, pp. 3594–3603.
- Fadhloun, K., and H. Rakha. A Novel Vehicle Dynamics and Human Behavior Car-Following Model: Model Development and Preliminary Testing. *International Journal of Transportation Science and Technology*, Vol. 9, No. 1, 2020, pp. 14–28.
- Makridis, M., G. Fontaras, B. Ciuffo, and K. Mattas. MFC Free-Flow Model: Introducing Vehicle Dynamics in Microsimulation. *Transportation Research Record: Journal of the Transportation Research Board*, 2019. 2673: 762–777.
- Fiori, C., V. Arcidiacono, G. Fontaras, M. Makridis, K. Mattas, V. Marzano, C. Thiel, and B. Ciuffo. The Effect of Electrified Mobility on the Relationship between Traffic Conditions and Energy Consumption. *Transportation Research Part D: Transport and Environment*, Vol. 67, 2019, pp. 275–290.
- Schakel, W. J., and B. van Arem. Improving Traffic Flow Efficiency by In-Car Advice on Lane, Speed, and Headway. *IEEE Transactions on Intelligent Transportation Systems*, Vol. 15, No. 4, 2014, pp. 1597–1606.
- Gipps, P. G. A Behavioural Car-Following Model for Computer Simulation. *Transportation Research Part B: Methodological*, Vol. 15, No. 2, 1981, pp. 105–111.
- Treiber, M., A. Hennecke, and D. Helbing. Congested Traffic States in Empirical Observations and Microscopic Simulations. *Physical Review E*, Vol. 62, No. 2, 2000, pp. 1805–1824.
- Brackstone, M., and M. McDonald. Car-Following: A Historical Review. *Transportation Research Part F: Traffic Psychology and Behaviour*, Vol. 2, No. 4, 1999, pp. 181–196.
- Helbing, D. Traffic and Related Self-Driven Many-Particle Systems. *Reviews of Modern Physics*, Vol. 73, No. 4, 2001, pp. 1067–1141.
- Cao, B., and Z. Yang. Car-Following Models Study Progress. *Proc., 2009 Second International Symposium on Knowledge Acquisition and Modeling*, Wuhan, China. 2009, pp. 190–193.
- Newell, G. F. A Simplified Car-Following Theory: A Lower Order Model. *Transportation Research Part B: Methodological*, Vol. 36, No. 3, 2002, pp. 195–205.
- Gazis, D. C., R. Herman, and R. W. Rothery. Nonlinear Follow-the-Leader Models of Traffic Flow. *Operations Research*, Vol. 9, No. 4, 1961, pp. 545–567.
- Searle, J. Equations for Speed, Time and Distance for Vehicles under Maximum Acceleration. *International Congress & Exposition*, Society of Automotive Engineers (SAE) -

- Advances in Safety Technology*, Detroit, MI, pp. 1–8, 1999. <https://doi.org/10.4271/1999-01-0078>.
- 18. Rakha, H. Validation of Van Aerde's Simplified Steady-state Car-Following and Traffic Stream Model. *Transportation Letters*, Vol. 1, No. 3, 2009, pp. 227–244.
 - 19. Rakha, H., I. Lucic, S. H. Demarchi, J. R. Setti, and M. V. Aerde. Vehicle Dynamics Model for Predicting Maximum Truck Acceleration Levels. *Journal of Transportation Engineering*, Vol. 127, No. 5, 2001, pp. 418–425.
 - 20. Rakha, H., and I. Lucic. Variable Power Vehicle Dynamics Model for Estimating Truck Accelerations. *Journal of Transportation Engineering*, Vol. 128, No. 5, 2002, pp. 412–419.
 - 21. Rakha, H., M. Snare, and F. Dion. Vehicle Dynamics Model for Estimating Maximum Light-Duty Vehicle Acceleration Levels. *Transportation Research Record: Journal of the Transportation Research Board*, 2004. 1883: 40–49.
 - 22. Rakha, H. A., K. Ahn, W. Faris, and K. S. Moran. Simple Vehicle Powertrain Model for Modeling Intelligent Vehicle Applications. *IEEE Transactions on Intelligent Transportation Systems*, Vol. 13, No. 2, 2012, pp. 770–780.
 - 23. Fadhloun, K., H. Rakha, A. Loulizi, and A. Abdelkefi. Vehicle Dynamics Model for Estimating Typical Vehicle Accelerations. *Transportation Research Record: Journal of the Transportation Research Board*, 2015. 2491: 61–71.
 - 24. Zhou, Q., J. Li, B. Shuai, H. Williams, Y. He, Z. Li, H. Xu, and F. Yan. Multi-Step Reinforcement Learning for Model-Free Predictive Energy Management of an Electrified Off-Highway Vehicle. *Applied Energy*, Vol. 255, 2019, p. 113755.
 - 25. He, Y., C. Wang, Q. Zhou, J. Li, M. Makridis, H. Williams, G. Lu, and H. Xu. Multiobjective Component Sizing of a Hybrid Ethanol-Electric Vehicle Propulsion System. *Applied Energy*, Vol. 266, 2020, p. 114843.
 - 26. European Commission. *A European Strategy for Low-Emission Mobility*, Brussels, Belgium, 2016.
 - 27. Ma, G., M. Ghasemi, and X. Song. Integrated Powertrain Energy Management and Vehicle Coordination for Multiple Connected Hybrid Electric Vehicles. *IEEE Transactions on Vehicular Technology*, Vol. 67, No. 4, 2017, pp. 2893–2899.
 - 28. Tian, Z., C. Zhang, and S. Zhang. Analytical Calculation of Magnetic Field Distribution and Stator Iron Losses for Surface-Mounted Permanent Magnet Synchronous Machines. *Energies*, Vol. 10, No. 3, 2017, pp. 1–12.
 - 29. Tsiakmakis, S., G. Fontaras, B. Ciuffo, and Z. Samaras. A Simulation-Based Methodology for Quantifying European Passenger Car Fleet CO₂ Emissions. *Applied Energy*, Vol. 199, 2017, pp. 447–465.
 - 30. Maurya, A. K., and P. S. Bokare. Study of Deceleration Behaviour of Different Vehicle Types. *International Journal for Traffic and Transport Engineering*, Vol. 2, No. 3, 2012, pp. 253–270.
 - 31. Treiber, M., and A. Kesting. Microscopic Calibration and Validation of Car-Following Models—A Systematic Approach. *Procedia: Social and Behavioral Sciences*, Vol. 80, 2013, pp. 922–939.
 - 32. Ciuffo, B., V. Punzo, and M. Montanino. Thirty Years of Gipps' Car-Following Model: Applications, Developments, and New Features. *Transportation Research Record: Journal of the Transportation Research Board*, 2012. 2315: 89–99.
 - 33. Schakel, W. J., B. van Arem, and B. D. Netten. Effects of Cooperative Adaptive Cruise Control on Traffic Flow Stability. *Proc., 13th International IEEE Conference on Intelligent Transportation Systems*, Funchal, Madeira Island, Portugal. IEEE. Piscataway, NJ, 2010, pp. 759–764.
 - 34. Wang, J., H. A. Rakha, and K. Fadhloun. Validation of the Rakha-Pasumarthy-Adjerid Car-Following Model for Vehicle Fuel Consumption and Emission Estimation Applications. *Transportation Research Part D: Transport and Environment*, Vol. 55, 2017, pp. 246–261.